Special Collection

The Sound of Batteries: An Operando Acoustic Emission Study of the $LiNiO_2$ Cathode in Li–Ion Cells

Simon Schweidler,[a] Matteo Bianchini,[a, b] Pascal Hartmann,[a, b] Torsten Brezesinski,*[a] and Jürgen Janek*[a, c]

The development of advanced Li-ion batteries relies on the implementation of high-capacity Ni-rich layered oxide cathode materials, such as NCM and NCA, among others. However, fast performance decay because of intrinsic chemical and structural instabilities hampers their practical application. Hence, thoroughly understanding degradation processes is crucial to overcome current limitations. To monitor instabilities of electrode materials under realistic operating conditions, the application of nondestructive *operando* techniques is required. While structural changes of crystalline phases can be studied by X-ray diffraction, microstructural changes (e.g., particle fracture) cannot be easily accessed *in situ* and are therefore mostly investigated *ex situ*. Here, we use acoustic emission (AE) measurements to probe a potential next-generation cathode material in real-time. Specifically, we focus on $LiNiO_2$ (LNO) and demonstrate that AE events in different frequency ranges can be correlated with the formation of the cathode solid-electrolyte interphase and the mechanical degradation during electrochemical cycling.

1. Introduction

Lithium nickel oxide ($LiNiO_2$, LNO) is an attractive cathode material for use in next-generation lithium-ion batteries (LIBs) because of its high theoretical specific capacity (~ 274 mAh g_{LNO}^{-1} below 4.3 V vs Li^+/Li).[1] Unfortunately, LNO exhibits mechanical, thermal and electrochemical instabilities during (de)lithiation. Most striking, it shows significant shrinkage in unit-cell volume upon charging. Especially the hexagonal H2→H3 phase transformation for lithium contents $x(Li) \leq 0.3$ causes a relative (anisometric) volume change of about −7% (total absolute relative volume change of ~9%).[1–3] The latter leads to inhomogeneous stress distribution and therefore to primary and secondary particle fracture.[4,5] This in turn results in side reactions between the freshly exposed surfaces and the electrolyte or to particle-particle contact loss. Such mechanical degradation phenomena, along with the dissolution of transition-metal ions and other structural changes, take place during cycling and negatively affect the capacity retention.[6–11]

X-ray diffraction (XRD),[10,12–18] differential electrochemical mass spectrometry (DEMS),[19–21] scanning electron microscopy (SEM),[17,18,22,23] transmission electron microscopy (TEM)[8,24–26] and X-ray photoelectron spectroscopy (XPS),[27–29] to name a few, are common analytical techniques to study the degradation of electrode materials in LIB cells. *Operando* XRD offers information on bulk volume changes in real-time, while crack formation is mostly observed *ex situ* by SEM or TEM. Hence, it is hardly possible to correlate the onset of mechanical degradation with the state of charge (SOC), i.e. with the electrochemical characteristics. However, it should be noted that there are some *operando* imaging techniques, such as tomography-based technologies.[30–33] For instance, the combination of *operando* and multi-scale X-ray computed tomography provided new insights into battery degradation and failure.[32]

Acoustic emission (AE) is a nondestructive technique that is widely used for monitoring fatigue, crack formation and mechanical damage in construction materials. In recent years, it has become a routine technology in structural health monitoring for the early detection of damages to bridges and in other concrete constructions.[34,35] More recently, AE has been used in the investigation of heterogeneous electrochemical processes, such as corrosion or anodization.[36–38] Consequently, it is not surprising that AE has also been applied to batteries. For instance, Kircheva *et al.* used AE to probe the solid-electrolyte

[a] S. Schweidler, Dr. M. Bianchini, Dr. P. Hartmann, Dr. T. Brezesinski, Prof. J. Janek
Battery and Electrochemistry Laboratory
Institute of Nanotechnology
Karlsruhe Institute of Technology (KIT)
Hermann-von-Helmholtz-Platz 1
76344 Eggenstein-Leopoldshafen, Germany
E-mail: torsten.brezesinski@kit.edu
juergen.janek@kit.edu
[b] Dr. M. Bianchini, Dr. P. Hartmann
BASF SE
Carl-Bosch-Strasse 38
67056 Ludwigshafen, Germany
[c] Prof. J. Janek
Institute of Physical Chemistry & Center for Materials Science
Justus-Liebig-University Giessen
Heinrich-Buff-Ring 17
35392 Giessen, Germany

Supporting information for this article is available on the WWW under https://doi.org/10.1002/batt.202000099

Special Collection An invited contribution to a joint Special Collection between Batteries & Supercaps and Chemistry–Methods on In Situ and Operando Methods for Energy Storage and Conversion.

interphase (SEI) formation and lithium intercalation into the bulk of graphite electrodes.[39] Moreover, Choe *et al.* analyzed damage mechanisms in lithium cobalt oxide ($LiCoO_2$, LCO) and graphite electrodes by classifying AE signals into distinct types,[40] and Villevieille *et al.* investigated conversion-type reactions in $NiSb_2$ electrodes.[41] Other LIB materials, such as silicon and metal hydrides, have also been studied; yet, Ni-rich layered oxide cathode materials have not been examined to date.[42–47]

It appears that virtually any process that is related to a minimum conversion of energy and local structural rearrangement emits sound. This makes AE not only a quite simple but also a highly sensitive and widely applicable tool. The downside of AE is the distinction and interpretation of the various acoustic events.

In the present work, we report a systematic study about the relationship between electrochemical performance, degradation and acoustic activity of LNO battery cells (with a lithium anode, so-called half-cells). To the best of our knowledge, this is the first *operando* AE study of LNO. Because LNO is an end-member of the lithium nickel cobalt manganese oxide (NCM) family, we consider it as a prototype material for the investigation of mechanical degradation in this group of cathodes.

2. Results and Discussion

As can be seen in Figure 1a, the cells showed the typical electrochemical trace for LNO, the voltage plateaus being associated with different phase transformations, as discussed elsewhere.[1,2,48] During the initial cycle in the voltage range between 3.0 and 4.3 V versus Li^+/Li, specific charge and discharge capacities of 258 and 228 mAh g_{LNO}^{-1} were achieved, corresponding to ~88% Coulombic efficiency (see also Figure S1 of the Supporting Information for the specific capacities in the first five cycles). In addition to the voltage profile, the cumulated hits and hit rate are also shown in Figure 1a. Major acoustic activity was detected during the first charge, which decreased in the following discharge. In the subsequent cycles, acoustic activity occurred only during charging. Because the initial charge was acoustically the most active, its AE characteristics are discussed in some more detail in the following.

First, a steady increase in acoustic activity up to ~3.8 V was observed (low-voltage region, referred to as LV, in Figure 1b). The acoustic activity then decreased slightly in the voltage range of 3.8–3.9 V and increased again in a rather linear fashion until the upper cutoff voltage was reached (high-voltage region, referred to as HV, in Figure 1b). The first strong increase (LV region) can probably be attributed to cathode SEI (cSEI) formation, as it has already been done in the case of graphite and LCO electrodes.[17,18] Based on both test measurements and literature data, a possible contribution of the lithium anode to the acoustic activity can be neglected (see Figure S2 of the Supporting Information).[39,49] Using electrochemical impedance spectroscopy (EIS), Zhan *et al.* suggested the successive formation/growth of cSEI layers with different properties: a

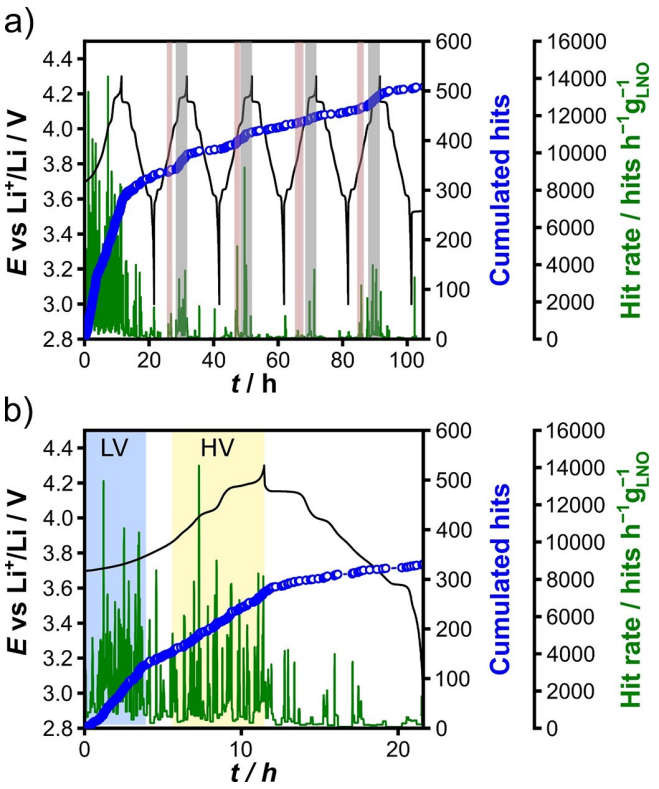

Figure 1. a) Voltage profile for the first five cycles of an LNO half-cell (black) and the corresponding cumulated hits (blue) and hit rate (green). Major increases in acoustic activity during the second to fifth cycles are highlighted for clarity. b) Enlarged view of the initial charge/discharge cycle. Low-voltage and high-voltage regions are denoted as LV and HV, respectively.

resistive layer followed by its conversion into a more conductive cSEI.[50,51] Hence, the further increase in acoustic activity from 3.9 to 4.3 V (HV region) may be explained by growth/conversion of the initial cSEI. However, it should be noted that the formation and composition of the passivating surface layer strongly depends on the type of electrolyte used.[52,53]

To provide evidence for the contribution of cSEI formation/conversion to the AE, EIS measurements were conducted on the LNO cells. During the first charge, the spectra (see Nyquist plots in Figure 2a and b) showed one or two semicircles and a straight slope at high/medium and low frequencies, respectively. We assign the high-frequency (HF) shift on the real *Z*-axis to the bulk electrolyte resistance (~5 Ω cm^2). An equivalent circuit is shown in Figure S3 of the Supporting Information. The HF semicircle represents the resistance and capacitance of the cSEI layer and the medium-frequency (MF) semicircle the charge-transfer resistance and double-layer capacitance. The low-frequency (LF) tail probably represents lithium diffusion in LNO.[54] The assembled (fresh) cell exhibited an initial resistance (HF semicircle) of ~70 Ω cm^2 (Figure 2a). After 3 h under open-circuit voltage (OCV) conditions, it had increased to ~160 Ω cm^2, indicating the formation of a resistive surface layer (upon contact between the LNO and the electrolyte) and its growth over time. After drawing current and direct increase in voltage to ~3.6 V (see Figure S4a of the Supporting Informa-

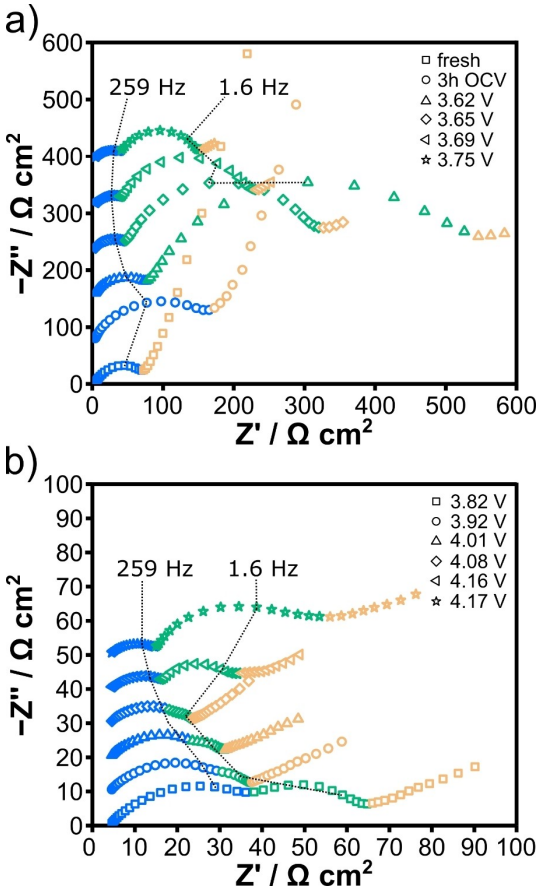

Figure 2. Nyquist plots of the electrochemical impedance for an LNO half-cell at different voltages during the initial charge cycle. a) Low-voltage and b) high-voltage regions. High- and medium-frequency semicircles and the low-frequency tail are shown in blue, green and orange, respectively. Data are offset along the imaginary *Z*-axis by 80 and 10 $\Omega\,cm^2$ in (a) and (b), respectively.

tion), a slight decrease of the HF semicircle as well as formation of a distinct MF semicircle were observed. As mentioned previously, the latter can be attributed to the charge-transfer resistance between the electrode and the electrolyte.[51,55] The decrease of the HF and MF semicircles afterwards indicates a change from an initially resistive to a more conductive cSEI layer.[50,51] Both semicircles decreased continuously as the first charge progressed, eventually causing them to merge, until a renewed increase of the MF semicircle at ~4.16 V occurred. The increase in resistance at high voltages is probably because of mechanical degradation and associated side reactions with the electrolyte.[56] This interpretation is supported by impedance measurements of the second charge cycle (see Figure S4b of the Supporting Information). In the second charge cycle, still a slight decrease in resistance was observed, before it increased again from ~4.16 V to the upper cutoff voltage, and an analogous formation of an MF semicircle as for the initial charge process occurred. We believe that the increase in resistance is due to the well-known collapse of the layered lattice structure. The latter is responsible for the generation of large mechanical stress, which may hinder lithium diffusion, and for the transition-metal migration, resulting in the formation of surface rock salt-like regions. Our impedance measurements show results for the cSEI formation comparable to the work of Zhang *et al.*[50,51] We therefore assume that the acoustic activity in the LV and HV regions is related to the mechanistically different formation of a resistive and a more conductive cSEI layer. Moreover, we suggest that the acoustic activity in the HV region is caused by mechanical processes, such as crack formation and crack propagation. LNO undergoes various phase transformations from hexagonal to monoclinic, H1→M, monoclinic to hexagonal, M→H2, and hexagonal to hexagonal, H2→H3 (see Figure S5 of the Supporting Information). It is known that the H2→H3 transformation at high voltages is mechanically most critical.[1,48,57] It has also been shown in literature that severe cracking already starts during the first charge and advances with cycling, eventually resulting in pulverization of the LNO secondary particles.[13,58]

To analyze the correlation between the detected AE events and their origin (cSEI formation, cracking etc.), the acoustic hits were sorted with respect to individual parameters. Each acoustic signal can generally be distinguished by its set of different characteristic parameters, such as duration, rise time, energy and amplitude, with the peak frequency appearing as the most distinctive AE parameter.[42,59]

Figure 3a depicts the peak frequency histogram of the AE signals detected in the first five cycles. Based on the histogram, we divided the acoustic hits into three groups. The first group, AE 1, covers a frequency range of 105–165 kHz, with a peak frequency maximum at 145 kHz. The second, AE 2, has a frequency range of 215–258 kHz, with a maximum number of hits at 245 kHz, and the third, AE 3, has a frequency range of 358–702 kHz, with a maximum at 435 kHz. By clustering the AE signals, the vast majority of AE 1 (~75%) and AE 2 hits (~74%) were detected during the first charge. The increase in the number of AE 1 and AE 2 hits acquired in the subsequent cycles was low compared to that for AE 3 (see Figure 3b and Figure S6 of the Supporting Information). Because the hits assigned to AE 1 and AE 2 occurred almost exclusively in the initial cycle, we believe that they are caused by cSEI formation, a process that usually takes place primarily during the initial charge.[54,60,61] In some case, hits in the frequency range AE 1 have been interpreted as the result of gas evolution. However, AE signals caused by gas evolution typically show long rise and duration times, which is not the case for AE 1 hits recorded here. In addition, de Biasi *et al.* demonstrated that CO_2 and O_2 evolve even at higher cycle numbers, especially in the H2 and H3 regions.[48] This in turn would mean that an increase in the number of AE 1 hits should also be expected to occur in the following cycles during charge and discharge. Moreover, SEM (next section) clearly showed formation of a passivating surface film. Together with the observation that the AE 1 hits decreased considerably after the initial cycle, this supports our assumption that the frequency range of AE 1 corresponds to cSEI formation. The same applies to the AE 2 hits, which according to literature lie at the border of acoustic activity between gassing and cracking.[40,42,59,62] Because the acoustic activity in the frequency range of AE 2 also decreased to a minor fraction after the initial cycle, we assign it to cSEI

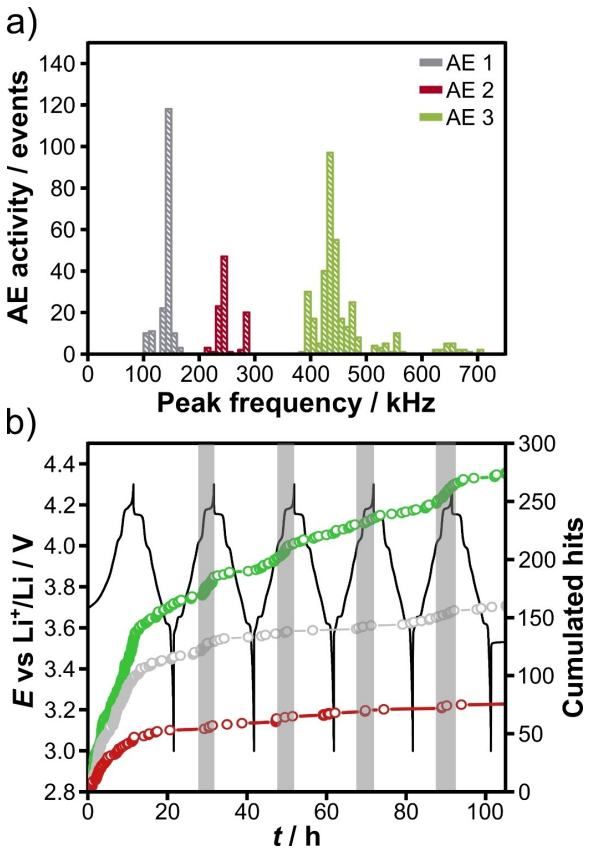

Figure 3. a) Peak frequency histogram of AE signals detected during the first five cycles. Signals were divided and clustered into three individual groups. b) Evolution of cell voltage and the corresponding cumulated hits for the different peak frequency ranges [color scheme as in (a)]. Major increases in acoustic activity during the second to fifth cycles are highlighted for clarity.

formation. Similar results that contradict the classical assignment of AE signals to gassing were observed in the investigation of silicon anodes and deposition of calcium carbonate and zinc phosphate.[42,63,64] In the case of silicon, acoustic activity due to gassing was excluded, as the other characteristic parameters of the individual signals did not fit those of gas evolution.

In the following cycles, a noticeable increase in acoustic activity (steps in the case of cumulative hits or sudden increase in hit rate) was observed particularly beyond the monoclinic phase for voltages above ~4.0 V (gray shaded areas in Figure 1a). The analysis also showed that the LV region of delithiation, in which a relative volume change of less than −2% occurs, has only a minor influence on the mechanical degradation (hardly any AE was detected here). This changed in the HV region, where a relative volume change of about −7% occurs, causing particle fracture and all the related side reactions.[48] A comparison of hits with the corresponding peak frequencies detected during the second to fifth cycles showed that hits are almost exclusively detected in the higher frequency range (see Figure 3b and Figure S6 of the Supporting Information). The high-frequency range of AE 3 can be assigned to intensive acoustic processes, especially to crack formation. This has been proven by different studies on various battery materials.[40,42,59,62,65–67] AE therefore provides evidence that mechanical degradation is mainly related to the occurrence of the hexagonal H2 and H3 phases in the case of LNO. We assume that both the above-mentioned second increase in hits in the initial cycle and the sudden increase in acoustic activity at high voltages in the following cycles are due to the induced strain and the associated degradation (fracture) behavior. It is also worth mentioning that in the further course of cycling, predominantly at high SOC, some (mostly minor) AE 1 and AE 2 events were detected, thereby indicating continuous cSEI formation (due to exposure of fresh reactive surfaces resulting from particle fracture, AE 3). We also note that hits of higher frequency (358–702 kHz) were detected over the entire voltage range upon charging in the first cycle. Clearly, AE monitoring supports the results on the degradation behavior of LNO (in the initial charge cycle) that have already been reported in literature.[1,13]

Moreover, an additional increase in acoustic activity in the voltage range of 3.75–3.95 V was detected in the second to fifth cycles, with the hit rate maximum varying slightly depending on the cycle number (red shaded areas in Figure 1a). This increase might be related to changes in the monoclinic phase of LNO. Using XRD, de Biasi *et al.* and others detected a splitting into the monoclinic 20–1 and 111 reflections when the voltage exceeds ~3.7 V.[48] For higher voltages, they observed convergence of the reflections with a minimum gap before they split again at 3.9 V. The resulting monoclinic distortion is mostly caused by lithium vacancy orderings.[48,68] Distortion of the monoclinic phase, which appears to generate considerable stress, would become visible in a measurable acoustic signal. In contrast to the charge cycles, only negligible numbers of AE events were observed in each discharge cycle.

An additional argument for the correct assignment of acoustic activity in AE 1 and AE 2 to surface-related degradation mechanisms was gained from *ex situ* SEM analysis. To this end, LNO cells were charged to different cutoff voltages and after opening in an Ar-filled glovebox, the cathodes were rinsed with dimethyl carbonate and then examined by SEM. The secondary particles showed spherical morphology with a size distribution of 8–10 μm; the primary particles had a size in the range between 200 and 400 nm (see Figure S7 of the Supporting Information). After drawing current, the initially smooth surface of the uncycled LNO (Figure 4a) showed a coarse but relatively uniform shell, the cSEI (Figure 4b). Accordingly, the imaging data in combination with the EIS results support our conclusion that the first increase in acoustic activity is because of cSEI formation (see also Figure S8 of the Supporting Information for high- and low-magnification SEM images recorded after charging to different voltages in the initial cycle).[39–41] This also corroborates indirectly our assumption that the AE detected beyond the monoclinic phase and up to the upper cutoff voltage is due to crack formation (Figure 4c and d), and this is further confirmed by direct comparison with the following cycles. In the second charge cycle, the already formed cSEI was clearly visible by SEM until ~3.8 V. Only for higher voltages (≥4.0 V), notable fracture of the primary and

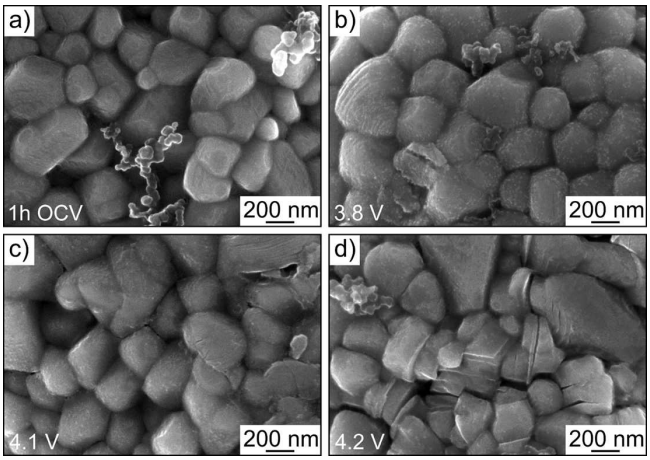

Figure 4. Top-view SEM images of the LNO cathode recorded after 1 h OCV (a) and after charging to ~3.8 (b), ~4.1 (c) and ~4.2 V (d) versus Li^+/Li in the initial cycle.

secondary particles was apparent (see Figure S9 of the Supporting Information).

It should be noted that the deposition of carbonate species on the surface of LNO might also cause acoustic emission.[63] CO_2 and O_2, among others, evolve during electrochemical decomposition of such surface contaminants, especially during the initial charge cycle. This has been shown for NCM cathode materials by Renfrew *et al.*[69] and Hatsukade *et al.*[20] using ^{18}O-labeled lithium transition-metal oxides and ^{13}C-labeled Li_2CO_3, respectively. To verify the possible influence of surface carbonate species on the AE measurement, LNO cathodes extracted at different voltages were investigated by acid titration (details in the Supporting Information). The cycling procedure was analog to the SEM study. Our results indeed indicate the presence of carbonate contaminants, which remained virtually unaltered during the first charge cycle (see Figure S10 of the Supporting Information). Further tests for a more detailed conclusion are still pending, but we exclude carbonate species as a source of AE at this time.

3. Conclusions

Acoustic emission is a suitable diagnostic tool to monitor the degradation of LNO upon (de)lithiation. The results are well reproducible and we were able to relate the different acoustic signals (hits) to different processes occurring during electrochemical cycling. The initial cycle was acoustically highly active because of cathode solid-electrolyte interphase formation and first excessive particle fracture. It was shown that crack formation and propagation, especially in the higher voltage region, have a profound effect on the acoustic activity during the first charge. In the further course, acoustic events were primarily detected in the range between ~4.0 and 4.3 V versus Li^+/Li. Based on the results from peak frequency analysis and *ex situ* SEM, acoustic emission in this voltage range can be attributed to additional cracking.

In summary, we conclude that acoustic emission offers independent and complementary experimental information on surface film formation, structural changes within the monoclinic phase range and mechanical degradation at high SOC. While different cathode materials may show different degradation mechanisms, our study demonstrates that acoustic emission is a promising nondestructive method for *operando* monitoring and probing electrode degradation and side reactions in battery cells. However, despite the simplicity of the experimental approach, unequivocal data interpretation remains challenging due to the complexity of the acoustic information.

Experimental Section

Materials and Testing

$LiNiO_2$ (LNO) was synthesized as described elsewhere.[48] Electrodes were prepared by slurry coating of 94 wt.% cathode material, 3 wt.% Super C65 carbon black additive (Timcal) and 3 wt.% Solef polyvinylidene fluoride binder (Solvay) in N-ethyl-2-pyrrolidone onto aluminum foil. The electrodes were dried over night at 100 °C in a vacuum and then calendared at 15 N/mm. Electrochemical testing was done on CR2032 coin cells. All cells were assembled in an Ar-filled glovebox (H_2O and O_2 < 0.1 ppm) and comprised an LNO cathode (~8.8 $mg_{LNO}\,cm^{-2}$), a GF/D glass microfiber separator (GE Healthcare Life Science, Whatman) and a lithium anode (Albemarle, Germany) of diameters 12, 17 and 15 mm, respectively. LP57 (200 µl) was used as electrolyte (BASF SE). The cells were cycled at C/10 rate (1 C = 225 mA g_{LNO}^{-1}) and 25 °C between 3.0 and 4.3 V versus Li^+/Li for five consecutive cycles using a BAT-SMALL potentiostat (Astrol Electronic AG).

Electrochemical impedance spectroscopy (EIS) was performed using a Bio-Logic VMP-3 potentiostat (Bio-Logic SAS). EIS data were acquired in the frequency range between 200 kHz and 10 mHz during galvanostatic intermittent titration technique (GITT) measurements. The coin cells were charged at C/10 rate and 25 °C for 1 h, followed by a 1 h rest step until the cutoff voltage of 4.3 V was reached. EIS was measured after cell assembly, after 3 h open-circuit voltage (OCV) period and after each rest step during cycling.

Acoustic Emission (AE)

The AE instrumentation consisted of a sensor, an in-line preamplifier and a data acquisition system (USB AE Node, MISTRAS Group, Inc.). To detect characteristic AE events, a differential wideband sensor with operating frequency range of 125–1000 kHz (MISTRAS Group, Inc.) was fixed using silicone grease to the coin cells on the LNO cathode side. The entire construction was placed inside a dense foam-box to decrease background noise from the laboratory. In all experiments, the preamp gain, analog filter and sampling rate were set to 40 dB, 20–1000 kHz and 5 MSPS, respectively. AE was recorded when a hit exceeded a threshold of 27 dB. In addition, the peak definition time, hit definition time and hit lockout time were set to 100, 200 and 200 µs, respectively. The recorded AE signals were processed with AEwin for USB software (MISTRAS Group, Inc.). Signals of less than two counts or lower than 100 kHz were eliminated. The sensor coupling was probed using the pencil-lead break test.[70] For the calculation of hit rate, the cumulated (measured) time-dependent AE signals were interpolated to an acquisition time with an interval of 10 s, differentiated and smoothed using a second order polynomial and 20 points per

window. For more details on the AE analysis, the reader is referred to literature.[39,42,43,59,71]

Scanning Electron Microscopy (SEM)

SEM data were acquired at 10 kV on a LEO-1530 instrument (Carl Zeiss AG, Oberkochen, Germany). An Ar-filled container was used for sample transfer from the glovebox to the microscope, with brief exposure to the ambient atmosphere during sample mounting onto the SEM stage.

Acknowledgements

The authors thank Jun Hao Teo for acid titration measurements, Dr. Katja Kretschmer and Dr. Florian Strauss for language editing and Christian Grupe for graphical assistance. This project was supported by BASF SE. Open access funding enabled and organized by Projekt DEAL.

Conflict of Interest

The authors declare no conflict of interest.

Keywords: lithium-ion battery · lithium nickel oxide · acoustic emission · cathode solid-electrolyte interphase · particle fracture

[1] M. Bianchini, M. Roca-Ayats, P. Hartmann, T. Brezesinski, J. Janek, *Angew. Chem. Int. Ed.* **2019**, *58*, 10434–10458.
[2] H. Li, N. Zhang, J. Li, J. R. Dahn, *J. Electrochem. Soc.* **2018**, *165*, A2985–A2993.
[3] J. Xu, F. Lin, M. M. Doeff, W. Tong, *J. Mater. Chem. A* **2017**, *5*, 874–901.
[4] L. de Biasi, G. Lieser, J. Rana, S. Indris, C. Dräger, S. Glatthaar, R. Mönig, H. Ehrenberg, G. Schumacher, J. R. Binder, H. Geßwein, *CrystEngComm* **2015**, *17*, 6163–6174.
[5] A. O. Kondrakov, A. Schmidt, J. Xu, H. Geßwein, R. Mönig, P. Hartmann, H. Sommer, T. Brezesinski, J. Janek, *J. Phys. Chem. C* **2017**, *121*, 3286–3294.
[6] E. M. Erickson, F. Schipper, T. R. Penki, J.-Y. Shin, C. Erk, F.-F. Chesneau, B. Markovsky, D. Aurbach, *J. Electrochem. Soc.* **2017**, *164*, A6341–A6348.
[7] S. M. Bak, E. Hu, Y. Zhou, X. Yu, S. D. Senanayake, S. J. Cho, K. B. Kim, K. Y. Chung, X. Q. Yang, K. W. Nam, *ACS Appl. Mater. Interfaces* **2014**, *6*, 22594–22601.
[8] F. Lin, I. M. Markus, D. Nordlund, T. C. Weng, M. D. Asta, H. L. Xin, M. M. Doeff, *Nat. Commun.* **2014**, *5*, 3529.
[9] R. Huang, Y. Ikuhara, *Curr. Opin. Solid State Mater. Sci.* **2012**, *16*, 31–38.
[10] L. de Biasi, A. O. Kondrakov, H. Geßwein, T. Brezesinski, P. Hartmann, J. Janek, *J. Phys. Chem. C* **2017**, *121*, 26163–26171.
[11] R. Jung, F. Linsenmann, R. Thomas, J. Wandt, S. Solchenbach, F. Maglia, C. Stinner, M. Tromp, H. A. Gasteiger, *J. Electrochem. Soc.* **2019**, *166*, A378–A389.
[12] L. de Biasi, B. Schwarz, T. Brezesinski, P. Hartmann, J. Janek, H. Ehrenberg, *Adv. Mater.* **2019**, *31*, 1900985.
[13] C. S. Yoon, D. W. Jun, S. T. Myung, Y. K. Sun, *ACS Energy Lett.* **2017**, *2*, 1150–1155.
[14] H. J. Noh, S. Youn, C. S. Yoon, Y. K. Sun, *J. Power Sources* **2013**, *233*, 121–130.
[15] A. O. Kondrakov, H. Geßwein, K. Galdina, L. de Biasi, V. Meded, E. O. Filatova, G. Schumacher, W. Wenzel, P. Hartmann, T. Brezesinski, J. Janek, *J. Phys. Chem. C* **2017**, *121*, 24381–24388.
[16] H. R. Kim, S. G. Woo, J. H. Kim, W. Cho, Y. J. Kim, *J. Electroanal. Chem.* **2016**, *782*, 168–173.
[17] S. Schweidler, L. de Biasi, G. Garcia, A. Mazilkin, P. Hartmann, T. Brezesinski, J. Janek, *ACS Appl. Energy Mater.* **2019**, *2*, 7375–7384.
[18] H. H. Ryu, K. J. Park, C. S. Yoon, Y. K. Sun, *Chem. Mater.* **2018**, *30*, 1155–1163.
[19] A. Schiele, B. Breitung, A. Mazilkin, S. Schweidler, J. Janek, S. Gumbel, S. Fleischmann, E. Burakowska-Meise, H. Sommer, T. Brezesinski, *ACS Omega* **2018**, *3*, 16706–16713.
[20] T. Hatsukade, A. Schiele, P. Hartmann, T. Brezesinski, J. Janek, *ACS Appl. Mater. Interfaces* **2018**, *10*, 38892–38899.
[21] P. Lanz, H. Sommer, M. Schulz-Dobrick, P. Novák, *Electrochim. Acta* **2013**, *93*, 114–119.
[22] P. Yan, J. Zheng, M. Gu, J. Xiao, J. G. Zhang, C. M. Wang, *Nat. Commun.* **2017**, *8*, 14101.
[23] D. J. Miller, C. Proff, J. G. Wen, D. P. Abraham, J. Bareño, *Adv. Energy Mater.* **2013**, *3*, 1098–1103.
[24] C. Liang, R. C. Longo, F. Kong, C. Zhang, Y. Nie, Y. Zheng, J.-S. Kim, S. Jeon, S. Choi, K. Cho, *J. Power Sources* **2017**, *340*, 217–228.
[25] S. Ahmed, A. Pokle, S. Schweidler, A. Beyer, M. Bianchini, F. Walther, A. Mazilkin, P. Hartmann, T. Brezesinski, J. Janek, K. Volz, *ACS Nano* **2019**, *13*, 10694–10704.
[26] H. Zhang, B. M. May, J. Serrano-Sevillano, M. Casas-Cabanas, J. Cabana, C. Wang, G. Zhou, *Chem. Mater.* **2018**, *30*, 692–699.
[27] T. Joshi, K. S. Eom, G. Yushin, T. F. Fullera, *J. Electrochem. Soc.* **2014**, *161*, A1915–A1921.
[28] H. Park, T. Yoon, Y. Kim, J. G. Lee, J. Kim, H.-s. Kim, J. H. Ryu, J. J. Kim, S. M. Oh, *J. Electrochem. Soc.* **2015**, *162*, A892–A896.
[29] J. Kim, H. Ma, H. Cha, H. Lee, J. Sung, M. Seo, P. Oh, M. Park, J. Cho, *Energy Environ. Sci.* **2018**, *11*, 1449–1459.
[30] E. H. R. Tsai, J. Billaud, D. F. Sanchez, J. Ihli, M. Odstrčil, M. Holler, D. Grolimund, C. Villevieille, M. Guizar-Sicairos, *iScience* **2019**, *11*, 356–365.
[31] D. P. Finegan, M. Scheel, J. B. Robinson, B. Tjaden, I. Hunt, T. J. Mason, J. Millichamp, M. Di Michiel, G. J. Offer, G. Hinds, D. J. L. Brett, P. R. Shearing, *Nat. Commun.* **2015**, *6*, 6924.
[32] D. P. Finegan, M. Scheel, J. B. Robinson, B. Tjaden, M. Di Michiel, G. Hinds, D. J. L. Brett, P. R. Shearing, *Phys. Chem. Chem. Phys.* **2016**, *18*, 30912–30919.
[33] M. Ebner, D. W. Chung, R. E. García, V. Wood, *Adv. Energy Mater.* **2014**, *4*, 1301278.
[34] C. Große, T. Schumacher, *Bautechnik* **2013**, *90*, 721–731.
[35] E. N. Landis, S. P. Shah, *J. Eng. Mech.* **1995**, *121*, 737–743.
[36] J. Tang, J. Li, H. Wang, Y. Wang, G. Chen, *Appl. Sci.* **2019**, *9*, 706.
[37] A. Yonezu, H. Cho, M. Takemoto, *Adv. Mater. Res.* **2006**, *13–14*, 243–249.
[38] M. Fregonese, H. Idrissi, H. Mazille, L. Renaud, Y. Cetre, *Corros. Sci.* **2001**, *43*, 627–641.
[39] N. Kircheva, S. Genies, D. Brun-Buisson, P.-X. Thivel, *J. Electrochem. Soc.* **2012**, *159*, A18–A25.
[40] C.-Y. Choe, W.-S. Jung, J.-W. Byeon, *Mater. Trans.* **2015**, *56*, 269–273.
[41] C. Villevieille, M. Boinet, L. Monconduit, *Electrochem. Commun.* **2010**, *12*, 1336–1339.
[42] A. Tranchot, A. Etiemble, P. X. Thivel, H. Idrissi, L. Roué, *J. Power Sources* **2015**, *279*, 259–266.
[43] A. Tranchot, H. Idrissi, P. X. Thivel, L. Roué, *J. Power Sources* **2016**, *330*, 253–260.
[44] A. Etiemble, H. Idrissi, S. Meille, L. Roué, *J. Power Sources* **2012**, *205*, 500–505.
[45] K. Rhodes, N. Dudney, E. Lara-Curzio, C. Daniel, *J. Electrochem. Soc.* **2010**, *157*, A1354–A1360.
[46] S. Kalnaus, K. Rhodes, C. Daniel, *J. Power Sources* **2011**, *196*, 8116–8124.
[47] C. Bommier, W. Chang, J. Li, S. Biswas, G. Davies, J. Nanda, D. Steingart, *J. Electrochem. Soc.* **2020**, *167*, 020517.
[48] L. de Biasi, A. Schiele, M. Roca-Ayats, G. Garcia, T. Brezesinski, P. Hartmann, J. Janek, *ChemSusChem* **2019**, *12*, 2240–2250.
[49] N. Kircheva, P.-X. Thivel, S. Genies, D. Brun-Buisson, Y. Bultel, *ECS Trans.* **2011**, *35*, 19–26.
[50] S. S. Zhang, K. Xu, T. R. Jow, *Electrochem. Solid-State Lett.* **2002**, *5*, A92–A94.
[51] S. S. Zhang, K. Xu, T. R. Jow, *J. Electrochem. Soc.* **2002**, *149*, A1521–A1526.
[52] D. Ostrovskii, F. Ronci, B. Scrosati, P. Jacobsson, *J. Power Sources* **2001**, *94*, 183–188.
[53] D. Aurbach, K. Gamolsky, B. Markovsky, G. Salitra, Y. Gofer, U. Heider, R. Oesten, M. Schmidt, *J. Electrochem. Soc.* **2000**, *147*, 1322–1331.
[54] J. Vetter, P. Novák, M. R. Wagner, C. Veit, K. C. Möller, J. O. Besenhard, M. Winter, M. Wohlfahrt-Mehrens, C. Vogler, A. Hammouche, *J. Power Sources* **2005**, *147*, 269–281.

[55] S. M. Choi, I. S. Kang, Y. K. Sun, J. H. Song, S. M. Chung, D. W. Kim, *J. Power Sources* **2013**, *244*, 363–368.
[56] E. Barsoukov, J. R. Macdonald, Impedance Spectroscopy: *Theory, Experiment, and Applications*, Second Edition, John Wiley & Sons, Inc., **2005**.
[57] W. Li, J. N. Reimers, J. R. Dahn, *Solid State Ionics* **1993**, *67*, 123–130.
[58] K. Dokko, M. Nishizawa, S. Horikoshi, T. Itoh, M. Mohamedi, I. Uchida, *Electrochem. Solid-State Lett.* **2000**, *3*, 125–127.
[59] N. Kircheva, S. Genies, C. Chabrol, P. X. Thivel, *Electrochim. Acta* **2013**, *88*, 488–494.
[60] M. B. Pinson, M. Z. Bazant, *J. Electrochem. Soc.* **2012**, *160*, A243–A250.
[61] G. Ning, B. Haran, B. N. Popov, *J. Power Sources* **2003**, *117*, 160–169.
[62] A. Etiemble, H. Idrissi, L. Roué, *J. Power Sources* **2011**, *196*, 5168–5173.
[63] S. Ramadan, H. Idrissi, *Desalination* **2008**, *219*, 358–366.
[64] F. Simescu, H. Idrissi, *Meas. Sci. Technol.* **2009**, *20*, 055702.
[65] A. Etiemble, P. Bernard, H. Idrissi, L. Roué, *Electrochim. Acta* **2015**, *186*, 112–116.
[66] S. Didier-Laurent, H. Idrissi, L. Roué, *J. Power Sources* **2008**, *179*, 412–416.
[67] E. Pomponi, A. Vinogradov, *Mech. Syst. Signal Process.* **2013**, *40*, 791–804.
[68] J. P. Peres, F. Weill, C. Delmas, *Solid State Ionics* **1999**, *116*, 19–27.
[69] S. E. Renfrew, B. D. McCloskey, *J. Am. Chem. Soc.* **2017**, *139*, 17853–17860.
[70] N. N. Hsu, Acoustic Emissions Simulator. US Patent 4,018,084, **1977**.
[71] A. Etiemble, H. Idrissi, L. Roue, *J. Acoust. Emiss.* **2012**, *30*, 54–64.

Manuscript received: May 7, 2020
Revised manuscript received: June 22, 2020
Accepted manuscript online: June 23, 2020
Version of record online: ■■, ■■■

ARTICLES

Battery beats: Acoustic emission is a versatile and nondestructive method for operando monitoring degradation of battery materials. Here, it is applied to probe in real-time the cathode active material $LiNiO_2$ (LNO) upon electrochemical cycling in lithium-ion cells.